

Damage evolution in Ti6Al4V–Al₃Ti metal–intermetallic laminate composites

Tiezheng Li^{a,b,*}, Fengchun Jiang^a, Eugene A. Olevsky^b, Kenneth S. Vecchio^a, Marc A. Meyers^a

^a Department of Mechanical and Aerospace Engineering, Materials Science and Engineering Program, University of California, San Diego, La Jolla, CA 92093-0411, USA

^b Department of Mechanical Engineering, San Diego State University, San Diego, CA 92182-1323, USA

Received 1 May 2006; received in revised form 5 May 2006; accepted 5 May 2006

Abstract

The crack propagation and damage evolution in metal (Ti6Al4V)–intermetallic (Al₃Ti) laminate composites were investigated. The composites (volume fractions of Ti6Al4V: 14%, 20% and 35%) were tested under different loading directions (perpendicular and parallel directions to laminate plane), to different strains (1%, 2%, 3%) and at different strain rates (0.0001 and 800–2000 s⁻¹). Crack densities and distributions were measured. The crack density increases with increasing strain, but decreases (at a constant strain) with increasing volume fraction of Ti6Al4V. Differences in crack propagation and damage evolution in MIL composites under quasi-static (10⁻⁴ s⁻¹) and dynamic (800–2000 s⁻¹) deformation were observed. The fracture stress does not exhibit significant strain-rate sensitivity; this is indicative of the dominance of microcracking processes in determining strength. Generally, the crack density after dynamic deformation is higher than that after quasi-static deformation. This is attributed to the decreased time for crack interaction in high-strain rate deformation. The effect of crack density, as quantified by a damage parameter, on elastic modulus and stress–strain relation were calculated and compared with experimental results.

© 2006 Elsevier B.V. All rights reserved.

Keywords: Laminate composites; Mechanical behavior; Damage evolution; Crack density

1. Introduction

Intermetallics are phases or compounds formed from constituent metals whose crystal structures are different from the individual metals, typically in an ordered atomic distribution or superlattice where the different atomic species occupy different regular lattice sites. As a distinct class of materials, intermetallics have good high-temperature strength, high resistance to oxidation and corrosion, high melting point, high stiffness, good creep resistance and relatively low density. Most intermetallics, however, exhibit brittle fracture and low tensile ductility at ambient temperature, because of limited dislocation mobility, insufficient number of slip or twinning systems and very low surface energy resulting in little to no plastic deformation at the crack tip. Their usefulness as engineering materials is, therefore, restricted in many cases by the poor fracture resistance and limited fabricability. In addition, a number

of them are sensitive to moisture in the environment at lower temperatures.

While many researchers have focused on the deformation mechanisms and the brittle fracture properties of intermetallics, others have concentrated on improving their mechanical and fracture properties by controlling microstructures, adding additional reinforcement phases and optimizing the processing variables [1–7]. As a result of those intense efforts, a number of new intermetallics based on nickel, iron and titanium and enhanced by reinforcement phases, in the form of particles [8–10], fibers [11–13] and layers [14–20], have been developed. Many of them provide very attractive mechanical and fracture properties for structural and aerospace applications. By optimizing the constituent properties in the layered structure, ductile reinforced intermetallic laminate composites improve the ductility necessary for intermetallics at low temperature, and in general, provide the maximum toughening efficiency among other forms of ductile reinforcements [21].

A number of diverse brittle intermetallics–ductile metal laminates have been produced, including Ti–Al₃Ti [22], Nb–Cr₂Nb [18], Nb–Nb₃Al [2], TiAl–TiNb [23], FeAl–TiC [24], Al–Al₂O₃

* Corresponding author. Tel.: +1 619 534 4719; fax: +1 619 534 5698.
E-mail address: mameyers@ucsd.edu (T. Li).

[25–27], $\text{Al}_2\text{O}_3\text{--Cu}$ [6], Al--NiAl [28], Mo--NiAl [29]. Among these laminate composites, the $\text{Ti6Al4V--Al}_3\text{Ti}$ laminate, fabricated from Ti6Al4V and Al foils by reaction synthesis in open air, has a great technological advantage and attracts special attention [30–32]. Previous works [22,30,31] have investigated the mechanical and fracture properties of $\text{Ti6Al4V--Al}_3\text{Ti}$ laminate composites, and proposed several models of crack propagation. This contribution, by experimentally establishing crack densities in the $\text{Ti6Al4V--Al}_3\text{Ti}$ laminate composites under different loading directions, strains, strain rates and volume fraction of constituents, seeks to provide a better understanding of damage evolution in this composite and its effect on the mechanical response.

2. Experimental procedure

The $\text{Ti6Al4V--Al}_3\text{Ti}$ MIL composites were processed by a novel one-step process in open air [30], stacking the alternating Ti6Al4V alloy and 1100-0 aluminum (see Table 1) foils and fabricating them in the synthesis apparatus with controlled tem-

Table 1
Chemical composition and mechanical properties of foil materials

Materials	Chemical composition (%)	Mechanical properties
Titanium Ti-6Al-4V	Ti: 89.57, Al: 6.13, C: 0.01 Fe: 0.1, H: 0.008, O: 0.16 N: 0.007, V: 4.01, Y: 0.005	Ultimate: 1035 MPa Yield: 950 MPa
Aluminum Al-1100-0	Al: 99, Cu: 0.05-0.2 Zn: 0.1, Mn: 0.05 Si and Fe: 0.95 All others: 0.05	Ultimate: 90 MPa

perature and pressure. The thickness of the initial Al and Ti alloy sheets is selected in such a manner that aluminum is completely consumed in forming the intermetallic compound Al_3Ti with alternating layers of partially unreacted Ti alloy.

The mechanical tests were conducted on rectangular samples with typical dimensions of $10\text{ mm} \times 8.5\text{ mm} \times 7.5\text{ mm}$ ($L \times W \times H$). Each curve represents the average of three to four tests. Samples were ground before testing, from 220 to 4000

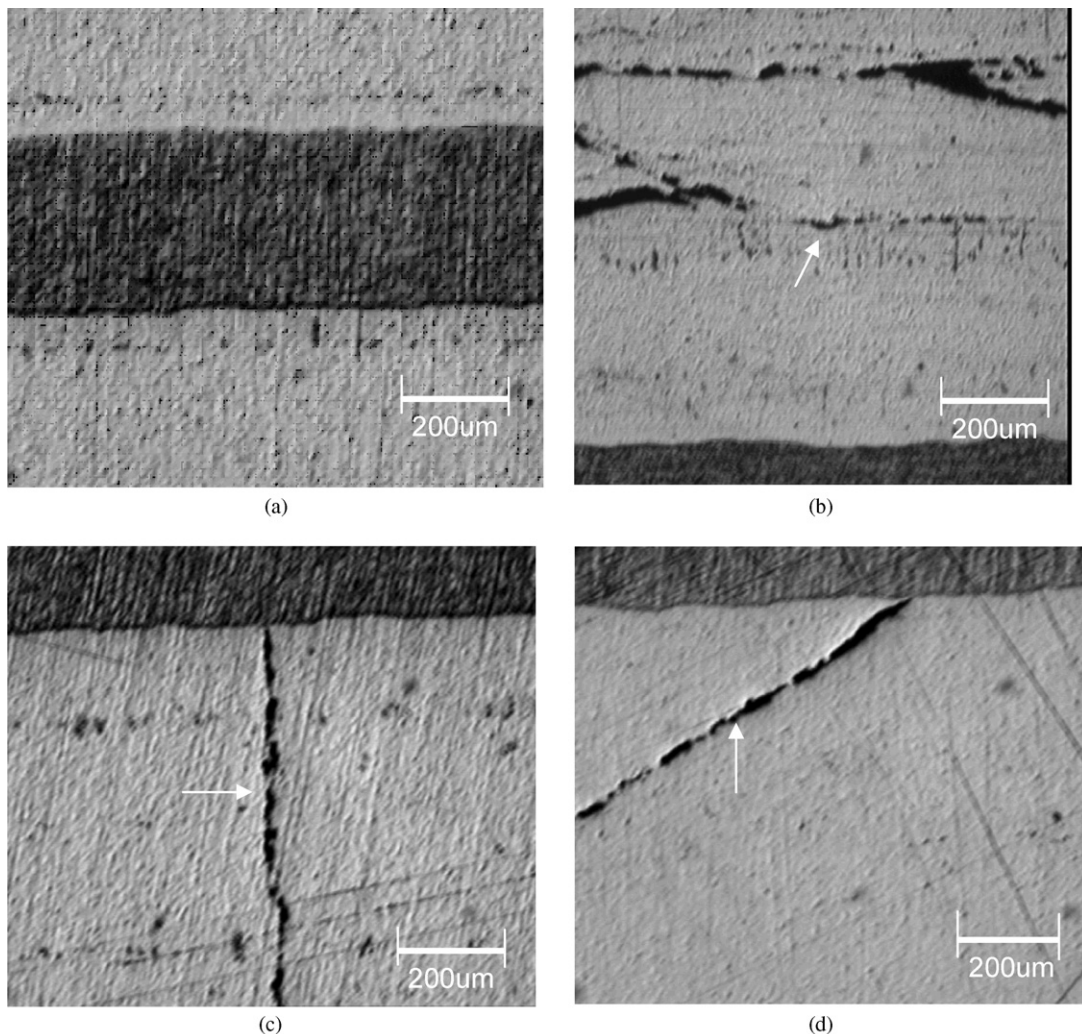


Fig. 1. Optical observations of untested $\text{Ti6Al4V--Al}_3\text{Ti}$ MIL composites: (a) typical optical picture; (b) crack parallel to the interface; (c) crack perpendicular to the interface; (d) crack inclined 45° to the interface.

grit, and then final polished by 0.05 μm Al_2O_3 in order to prevent the variation of surface damage characteristics, which may occur if polished after testing. Quasi-static compression tests were performed at a strain rate of 10^{-4} s^{-1} on a SATEC testing frame, and dynamic compression tests were performed at strain rates in the range of 800–2000 s^{-1} in a split Hopkinson pressure bar. The mechanical tests were conducted in both perpendicular and parallel directions to the metal-intermetallic interfaces, for different volume fractions of Ti6Al4V (14%, 20% and 35%) and to different strains ($\sim 1\%$, $\sim 2\%$, $\sim 3\%$ and failure strains). The specimens were then observed under a FEI Quanta 600 scanning electron microscope to characterize the cracking and damage evolution.

Optical microscopy was used to investigate the crack morphology in the as-processed Ti6Al4V– Al_3Ti MIL composites. Rectangular specimens of 80 mm \times 18 mm \times 8 mm were used to minimize the edge effect on the crack distribution and to ensure the statistical validity. The samples were ground from 220 to 4000 grit, and then final polished by 0.05 μm Al_2O_3 . A Nikon Epiaphot optical microscope and Image-Pro Plus image analysis software were used to digitally store and analyze the images. The crack location, crack orientation, crack number and crack density before and after testing were measured.

3. Results and discussion

3.1. Cracks in as-processed samples

The as-processed samples contained cracks, whose nature and source will be presented in a future report [33]. Fig. 1(a) shows a typical optical observation of the as-processed Ti6Al4V– Al_3Ti MIL composite. The darker phase is Ti6Al4V and the lighter one is Al_3Ti . Most cracks are located in the Al_3Ti layers. They can be classified into three types: parallel to the interface, perpendicular to the interface and inclined ($\sim 45^\circ$) to the interface. They are also described by Li et al. [22]. Fig. 1(b)–(d) show the optical observations of those three typical configurations.

Photomicrographs were taken for the entire specimen and assembled in montages. Figs. 2–4 show the montages for different volume fractions of Ti6Al4V: 14%, 20% and 35%. All cracks (parallel, perpendicular and inclined ($\sim 45^\circ$) to the interface) were measured for the three composites. Figs. 5–7 show the crack distribution for the three as-processed MIL composites. In all cases, the length of perpendicular cracks is close to the average thickness of Al_3Ti layers, and the length of inclined cracks is close to $\sqrt{2}$ times of the average Al_3Ti layer. Tables 2 and 3 summarize the crack distribution and crack density measurements.

Table 2
Crack sizes and density in as-processed MIL composites

	Perpendicular (μm)	Inclined (μm)	Al_3Ti thickness (μm)	Crack density (mm/mm^2)
14% Ti6Al4V	900–1150	1400	1000	0.321
20% Ti6Al4V	660–740	1000	700	0.255
35% Ti6Al4V	340–480	600	450	0.137

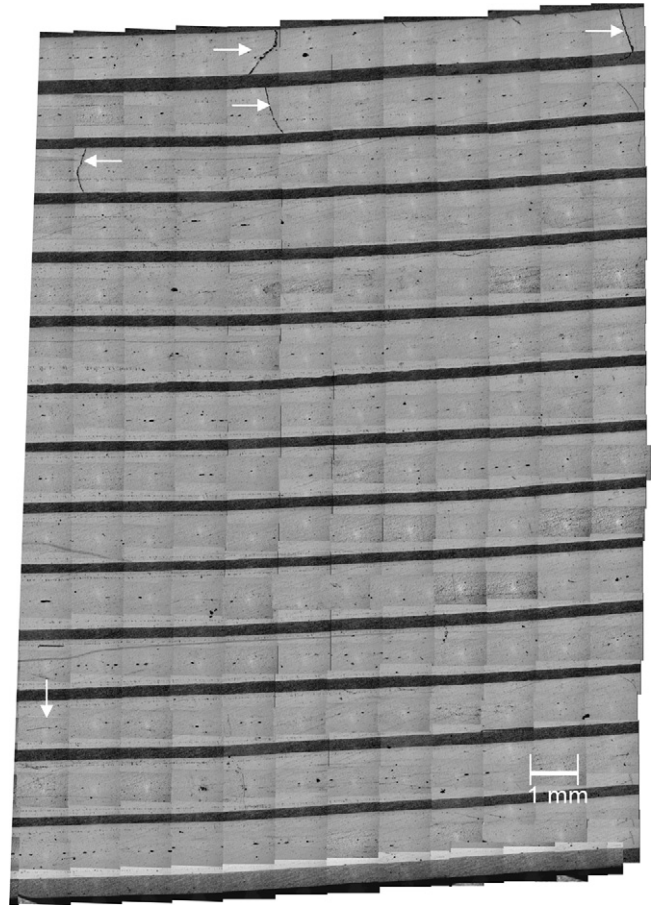


Fig. 2. A montage of part of the cross-section of as-processed 14% Ti6Al4V MIL composite (cracks marked by arrows).

Table 3
Crack distribution in as-processed MIL composites

	Perpendicular (%)	Inclined (%)	Parallel (%)
14% Ti6Al4V	49	31	20
20% Ti6Al4V	59	19	22
35% Ti6Al4V	72	7	21

The crack density, ρ_{crack} was calculated by dividing the total length of cracks, ℓ , by the total surface area they are located, A .

$$\rho_{\text{crack}} = \frac{\ell}{A} \quad (1)$$

The second dimension of the crack is not known and is assumed to be equal to the thickness of the specimen, t . It is possible that the sample size has an effect on this value. The crack

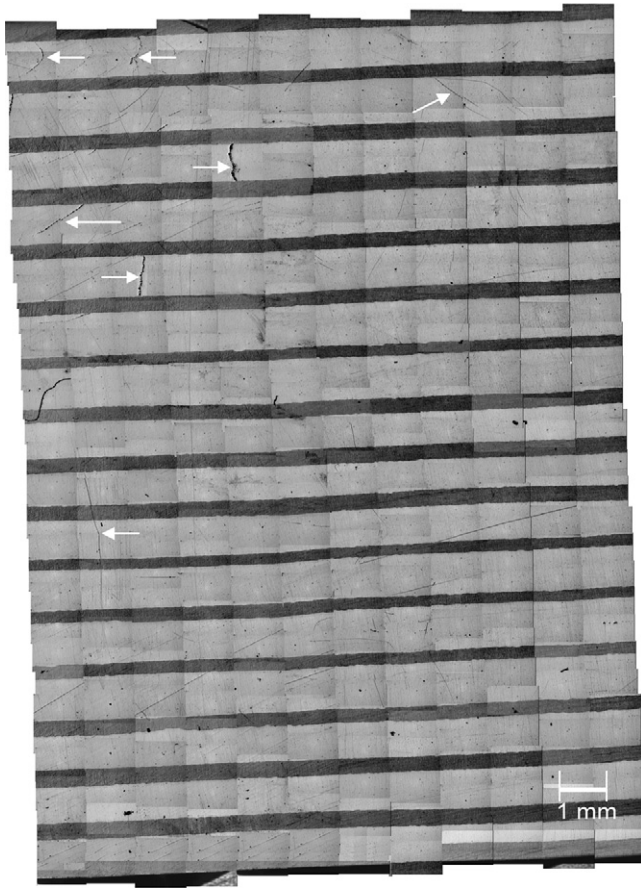


Fig. 3. A montage of part of the cross-section of as-processed 20% Ti6Al4V MIL composite (cracks marked by arrows).

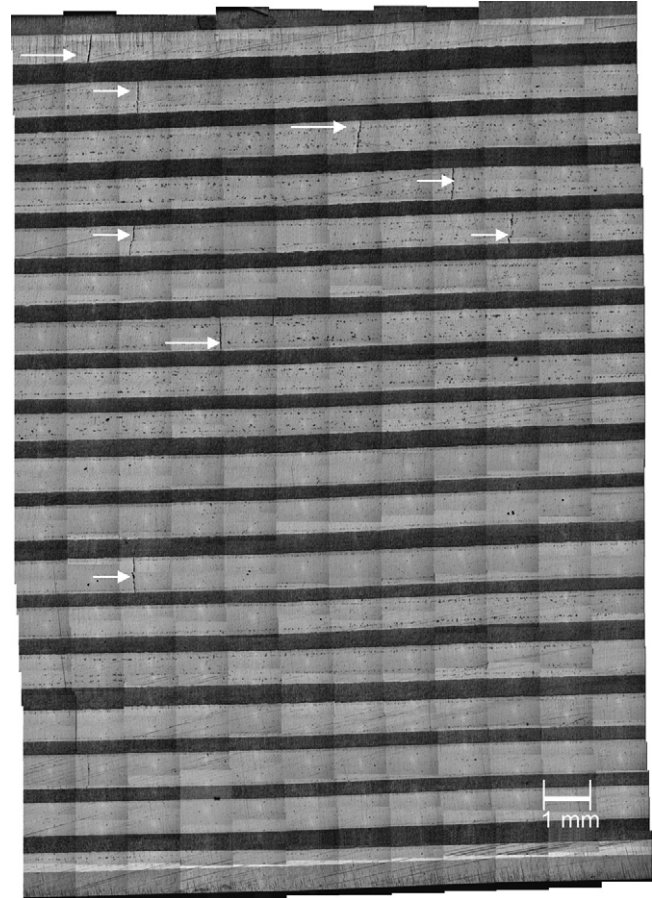


Fig. 4. A montage of part of the cross-section of as-processed 35% Ti6Al4V MIL composite (cracks marked by arrows).

density, represented as the area of cracks per unit volume, is

$$\rho_{\text{crack}} = \frac{lt}{At} = \frac{lt}{V} \quad (2)$$

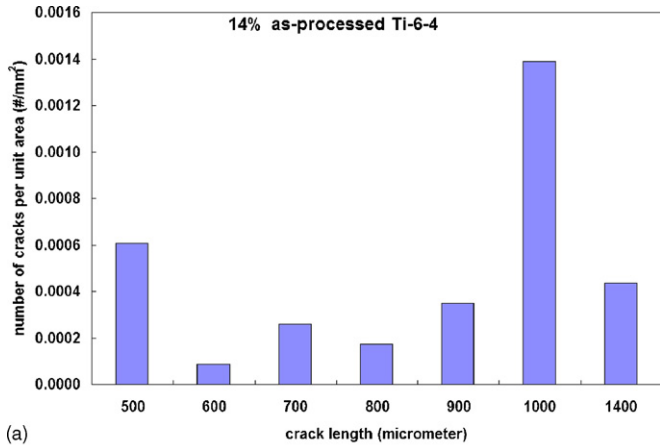
Fig. 8 shows the comparison of crack density and the percentage of different types of crack orientation in 14%, 20% and 35% as-processed composites. With increasing volume fraction of Ti6Al4V, the crack density decreases from 0.321–0.255 to 0.137 mm/mm². Because of the thermal mismatch between Ti6Al4V and Al₃Ti, the residual stress accumulates during the cooling process and renders the Al₃Ti layers under tension and Ti6Al4V layers under compression. A smaller volume fraction of Ti6Al4V produces larger residual stress in the brittle Al₃Ti layers, and thus forms more cracks and results in a larger crack density. This will be analytically described in a forthcoming report [33]. Fig. 8(b) shows the crack distributions. It is seen that while the concentration of parallel cracks tends to be consistent across volume fractions of Ti6Al4V, the concentration of perpendicular cracks increases from 49% (14% Ti6Al4V) to 72% (35% Ti6Al4V) and the concentration of inclined cracks decreases from 31% (14% Ti6Al4V) to 7% (35% Ti6Al4V). This means that although the number of overall cracks decreases with increasing volume fraction of Ti6Al4V, the number of perpendicular cracks decreases relatively less than the number of inclined cracks and the percentage of perpendicular cracks increases at the expense of the inclined cracks.

3.2. Damage evolution in Ti6Al4V–Al₃Ti MIL composites

3.2.1. Quasi-static compression tests (0.0001 s⁻¹): parallel to the interface

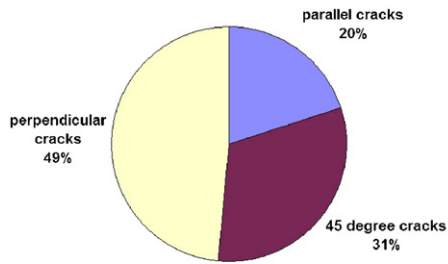
Fig. 9 shows the SEM pictures of 14%, 20% and 35% MIL composites after quasi-static loading in parallel direction. At ~1% strain (Fig. 9(a), (c) and (e)), the basic layered structure of Ti6Al4V–Al₃Ti is maintained, while most cracks are parallel cracks in the middle of the Al₃Ti layer. At the failure strain (Fig. 9(b), (d), (f) and (g)), delamination along the interface, parallel cracks in the middle of the Al₃Ti layers, as well as buckling of Ti6Al4V layers, are observed. The inclined cracks in Al₃Ti are occasionally seen but soon re-align themselves in the loading directions, connecting the cracks along the interfaces and the cracks along the middle of the Al₃Ti or connecting cracks along the interfaces in the opposite side of the Al₃Ti layer (Fig. 9(i)).

As Fig. 9 shows, cracks in Al₃Ti layer develop at ~1% strain and most of the cracks are along the middle of the Al₃Ti layers, where is typical weaker than the rest of composites and usually consists of a combination of voids, impurity and the reaction residue. As the strain increases, these cracks continue to develop and delaminations occurs. The inclined cracks are rare, but when they develop, they have the tendency to re-align in the loading direction and connect the other parallel cracks.



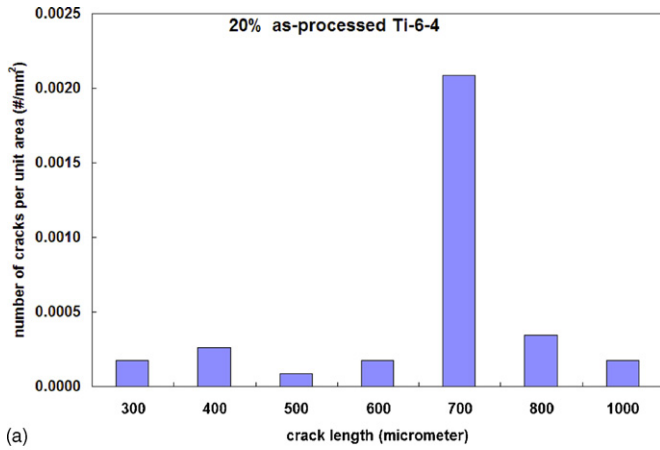
(a)

14% as-processed Ti-6-4



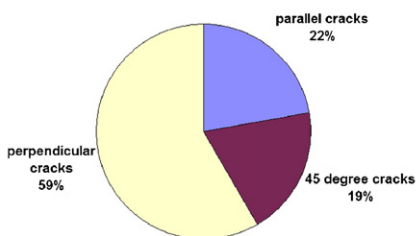
(b)

Fig. 5. Crack distribution of as-processed 14% Ti6Al4V MIL composite.



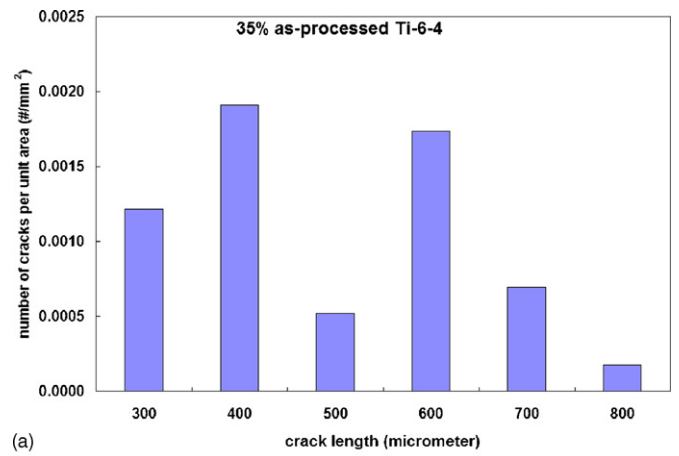
(a)

20% as-processed Ti-6-4



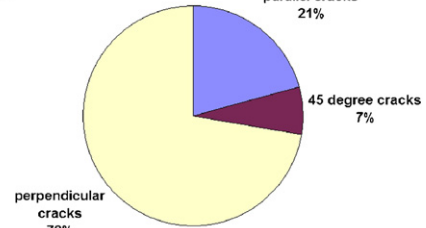
(b)

Fig. 6. Crack distribution of as-processed 20% Ti6Al4V MIL composite.



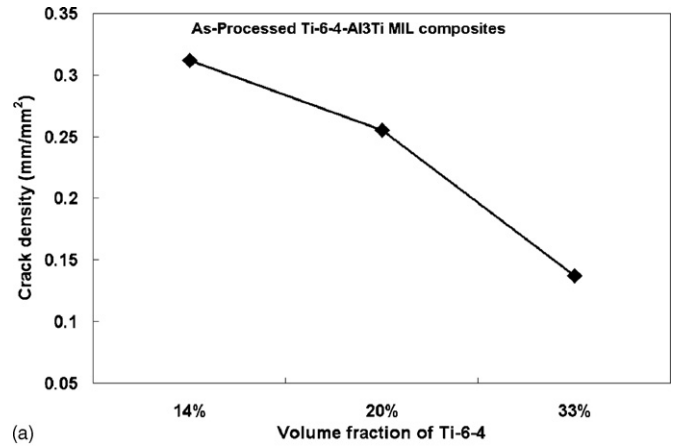
(a)

35% as-processed Ti-6-4

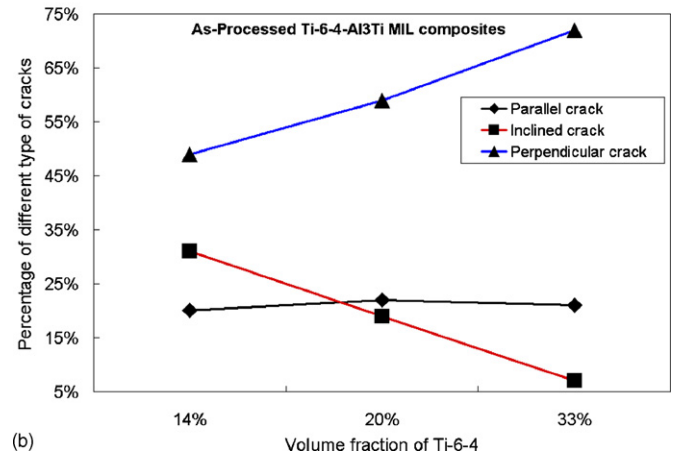


(b)

Fig. 7. Crack distribution of as-processed 35% Ti6Al4V MIL composite.



(a)



(b)

Fig. 8. Crack densities and percentage of different types of crack orientations in 14%, 20% and 35% MIL composites.

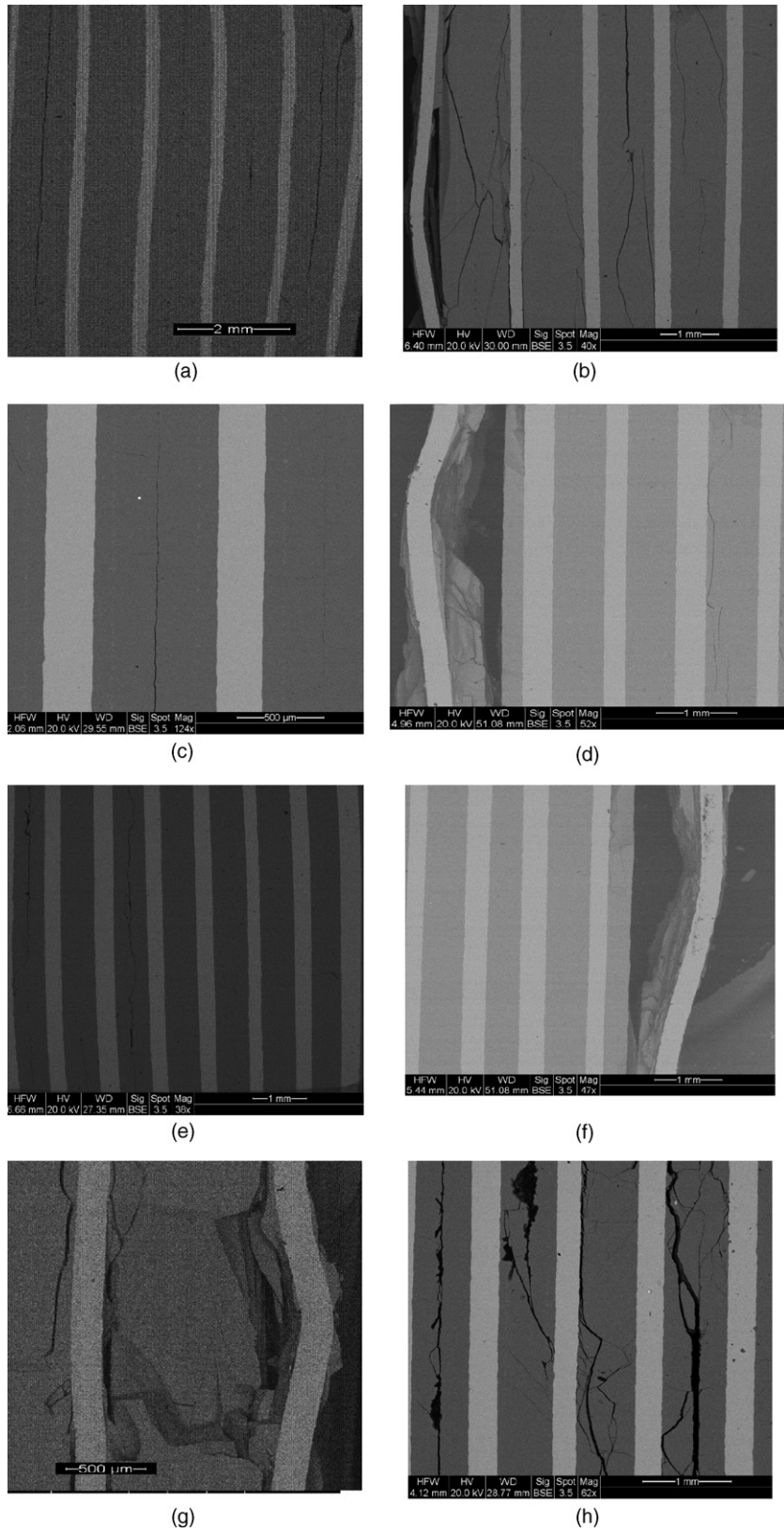


Fig. 9. SEM of MIL composites after quasi-static compression in parallel loading: (a) 14% Ti6Al4V, 1% strain; (b) 14% Ti6Al4V, 1.7% (failure); (c) 20% Ti6Al4V, 1% strain; (d) 20% Ti6Al4V, 2.3% (failure); (e) 35% Ti6Al4V, 1% strain; (f) 35% Ti6Al4V, 2.9% (failure); (g) 14% Ti6Al4V, 1.7% (failure); (h) 20% Ti6Al4V, 2.3% (failure).

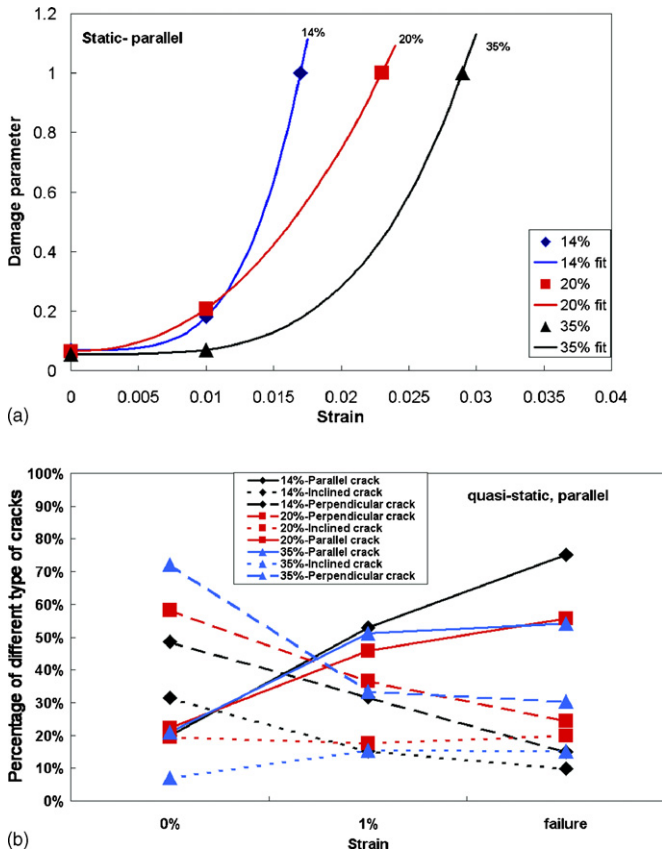


Fig. 10. Crack densities and crack distributions for MIL composites after quasi-static compression in parallel loading: (a) damage parameter; (b) crack distribution.

The mechanism is discussed by Li et al. [22]. When the Al_3Ti layers fail, the $\text{Ti}_6\text{Al}_4\text{V}$ layers take the additional loading and have the tendency to buckle. Because the strength of the composites increases with increasing volume fraction of $\text{Ti}_6\text{Al}_4\text{V}$, the composites with higher volume fraction of $\text{Ti}_6\text{Al}_4\text{V}$ fail at higher strains. However, the major features of failure in parallel loading are similar: delamination along the interfaces, buckling of $\text{Ti}_6\text{Al}_4\text{V}$ layers and cracking in the middle of the Al_3Ti layers.

It is possible to convert the crack density into a damage parameter, D , which is defined as a measure of the physical damage in materials. When $D=0$, one has a material state with no damage; D increases with damage progression until it reaches 1 when the material fails. The advantage of using D is that it is a unitless number, and can be calculated as:

$$D = \frac{A_c}{A} = \frac{m\pi a^2}{A} = \frac{\pi A \rho_{\text{crack}}^2}{4m} \quad (3)$$

where A_c is the effective damage area assumed to be, in this section, of a region in which the crack is located, A the total surface area, a one half of the crack length, ρ_{crack} the crack density defined in Eq. (1) and m is the total number of cracks. Here, we assume that the dimension of the cracks perpendicular to the surface is equal to the thickness of specimen, and that cracks propagate unimpeded through the Al_3Ti . Fig. 10 shows the damage parameter, D , and crack distribution for 14%, 20%

and 35% MIL composites at increasing strains. A power-law relation between D and ε is employed to fit the experimental data:

$$D = D_0 + k\varepsilon^n \quad (4)$$

where D_0 , n and k are material parameters. As the strain increases, D increases; at a constant strain, damage increases with decreasing concentration of $\text{Ti}_6\text{Al}_4\text{V}$. The damage parameter increases to unity at failure (Fig. 10(a)). As the strain increases, the concentration of the parallel cracks overtakes that of the perpendicular and inclined cracks as the major crack morphology. The concentration of parallel cracks increases sharply from 0% to 1% strain and then more gradually until failure (Fig. 10(b)).

3.2.2. Dynamic compression tests: parallel to the interface

Because of the difficulty of controlling the strains under dynamic loading, only specimens at $\sim 1\%$ strain and failure were obtained.

Fig. 11 shows the SEM pictures of 14%, 20% and 35% MIL composites after dynamic loading in parallel direction with $800\text{--}2000\text{ s}^{-1}$ strain rates. At $\sim 1\%$ strain (Fig. 11(a), (c) and (e)), although the basic layered structure of $\text{Ti}_6\text{Al}_4\text{V}\text{--}\text{Al}_3\text{Ti}$ is retained, larger damage is observed than in Fig. 9. Cracks are formed along the middle of the Al_3Ti layer, parallel and perpendicular to the interfaces. At failure (Fig. 11(b), (d) and (f)), the cracks developed at $\sim 1\%$ strain continue to grow, leading to the buckling of $\text{Ti}_6\text{Al}_4\text{V}$ layers and delamination along the interfaces and along the middle of the Al_3Ti layers. An interesting feature after dynamic loading in parallel direction is that many Al_3Ti layers are blown away upon impact, even at $\sim 1\%$ strain; at failure, only part of the Al_3Ti layers are retained, with the left Ti layers, seen in the secondary electron micrograph (Fig. 11(h) and (i)). It is also observed in some specimens that only half of Al_3Ti is left in through the thickness (Fig. 11(b) and (h)).

From Fig. 11, the cracks along the middle of the Al_3Ti layers are most common at $\sim 1\%$ strain. Because the impact process was completed in such a short period of time, the severely deformed Al_3Ti would not be accommodated in the existing structure, and many were blown away (Fig. 11(g)). This significantly weakens the intermetallic phase, and leaves Ti layers to take additional loading instantly. Finally, failure occurs, in the form of delamination along the interface and buckling of $\text{Ti}_6\text{Al}_4\text{V}$ layers. Comparing with quasi-static tests, the composites after dynamic tests are much more fragmented and many Al_3Ti layers are blown away upon impact. This leads to the simultaneous delamination of several interfaces, usually breaking the specimens into fragmented pieces. As this happens, each of those parts suddenly experiences a sharp increase in stress concentration, leading to severely damaged specimens.

Fig. 12 shows the damage parameter and crack distribution for 14%, 20% and 35% MIL composites at different strains after dynamic loading in parallel direction. It is seen that, as the strain increases, the damage parameter across volume fractions of $\text{Ti}_6\text{Al}_4\text{V}$ increases. In comparison with those after quasi-static loading in parallel direction, the damage parameters at

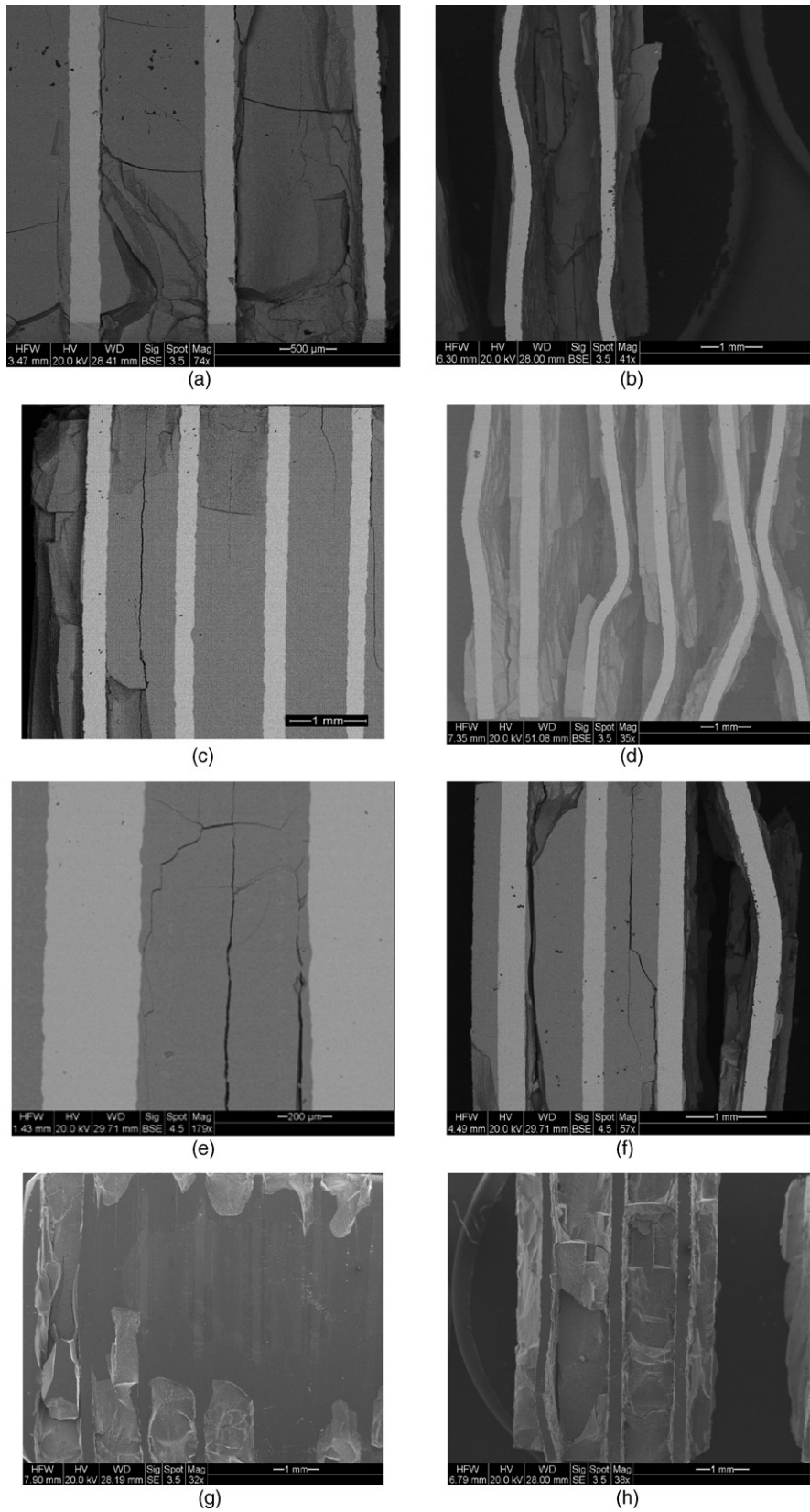


Fig. 11. SEM of MIL composites after dynamic compression in parallel loading: (a) 14% Ti6Al4V, ~1% strain; (b) 14% Ti6Al4V, ~1.9% (failure); (c) 20% Ti6Al4V, ~1% strain; (d) 20% Ti6Al4V, ~2.5% (failure); (e) 35% Ti6Al4V, ~1% strain; (f) 35% Ti6Al4V, ~3.3% (failure); (g) 14% Ti6Al4V, ~1%; (h) 14% Ti6Al4V, ~1.9% (failure).

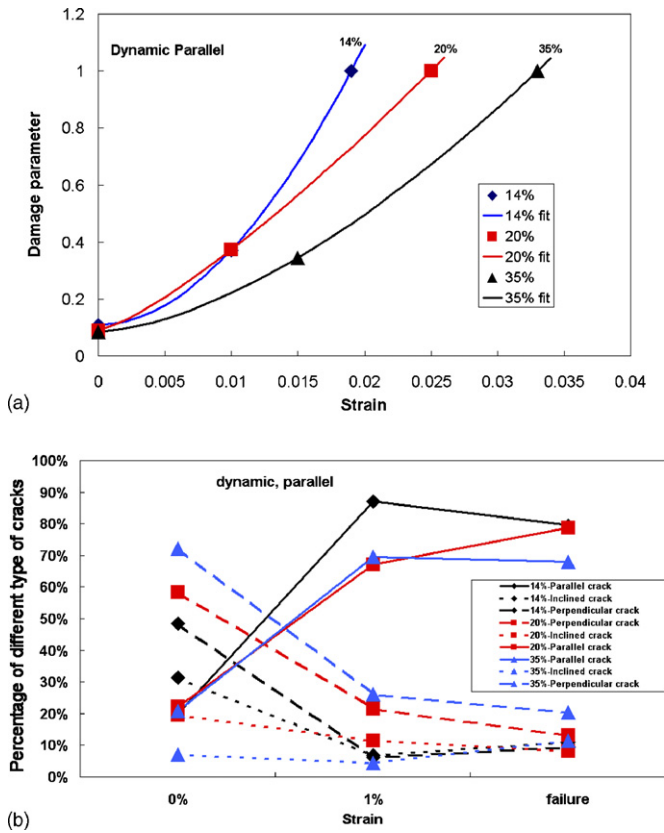


Fig. 12. Crack densities and crack distributions for MIL composites after dynamic compression in parallel loading: (a) damage parameter; (b) crack distribution.

~1% strain are higher, due to the severe damage upon impact. The concentration of the parallel cracks dominates among the different types of cracks, and is also larger than those after quasi-static parallel deformation.

Fig. 13 compares the crack density at ~1% strain and failure after dynamic and quasi-static loading in parallel direction. At ~1% strain, the crack densities in dynamic loading are higher than those in quasi-static loading. Because of the higher strength

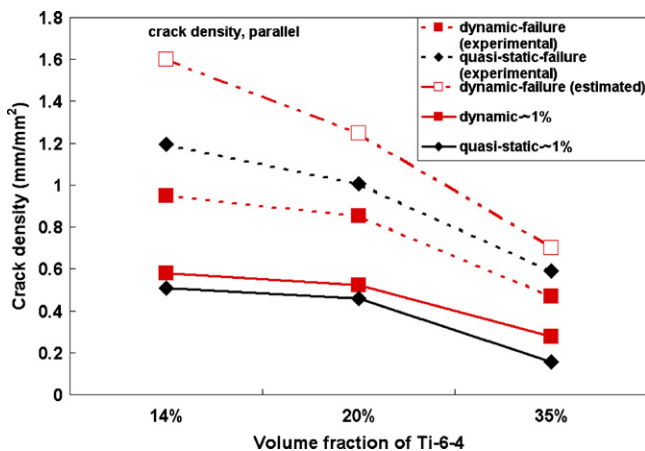


Fig. 13. Crack density comparison at ~1% and failure strain after the dynamic and quasi-static loading in parallel direction.

the added Ti6Al4V provides, the crack density decreases as the volume fraction of Ti6Al4V increases. At the failure, however, contrary to our expectation (that the crack densities in the dynamic conditions are higher than those in the quasi-static conditions), the data shows that the crack densities after dynamic parallel loading are lower than those after quasi-static parallel loading. One possible reason is that the specimens after dynamic loading up to failure are very fragmented, and most of time only parts of the specimens could be obtained. The data from those parts thus underestimated the crack density after dynamic parallel loading. The dotted line is the estimate of the real crack density after dynamic loading, which shows a decrease in crack density with increasing concentration of Ti6Al4V and the crack density after dynamic testing higher than that after quasi-static parallel loading.

3.2.3. Quasi-static compression tests (0.0001 s⁻¹): perpendicular to the interface

Fig. 14 shows the SEM pictures of 14%, 20% and 35% MIL composites after quasi-static loading in perpendicular direction. At ~1% strain (Fig. 14(a), (c) and (e)), the basic layered structure of Ti6Al4V–Al₃Ti is maintained, while cracks are in the form of perpendicular, parallel and inclined directions to the interfaces. At failure (Fig. 14(b), (d) and (f)), Ti6Al4V layers fail by the shear cracks, 45° to the interfaces. Also seen at failure are some parallel cracks along the middle of Al₃Ti layers and delamination along the interfaces. At the intermediate strains, shear band development is observed (Fig. 14(g): ~2% strain and (h): ~2.5% strain). In Fig. 14(g), the shear bands are in their early stages, when the inclined cracks reach the interfaces and plastically deform the Al₃Ti layers by squeezing further into Ti6Al4V layers. Fig. 14(h) shows the later stage of the shear band development, as the shear bands from the opposite side of the Al₃Ti layers start to reach for each other, forming shear cracks in Ti6Al4V layers. The cracks that reach the interface but do not develop shear bands in Ti6Al4V deviate along the interface and delaminate the Ti6Al4V–Al₃Ti interface.

Fig. 15 shows the damage parameter and crack distribution for 14%, 20% and 35% MIL composites of different strains after quasi-static loading in perpendicular direction. It is found that the damage parameter increases with increasing strains, and the increase accelerates approaching failure (Fig. 15(a)). The percentages of different types of cracks are stable with increasing strains, and the concentration of inclined cracks is slightly higher at failure (Fig. 15(b)).

3.2.4. Dynamic compression tests: perpendicular to the interface

Fig. 16 shows the SEM pictures of 14%, 20% and 35% MIL composites after dynamic loading in perpendicular direction with 800–2000 s⁻¹ strain rates. At ~1% strain (Fig. 16(a), (c) and (e)), similar to quasi-static tests, most cracks are aligned with the loading direction or along the middle of the Al₃Ti layers. At failure (Fig. 16(b), (d) and (f)), the Ti6Al4V layers are failed by the shear cracks, parallel cracks along the middle of the Al₃Ti layers and the delaminations along the

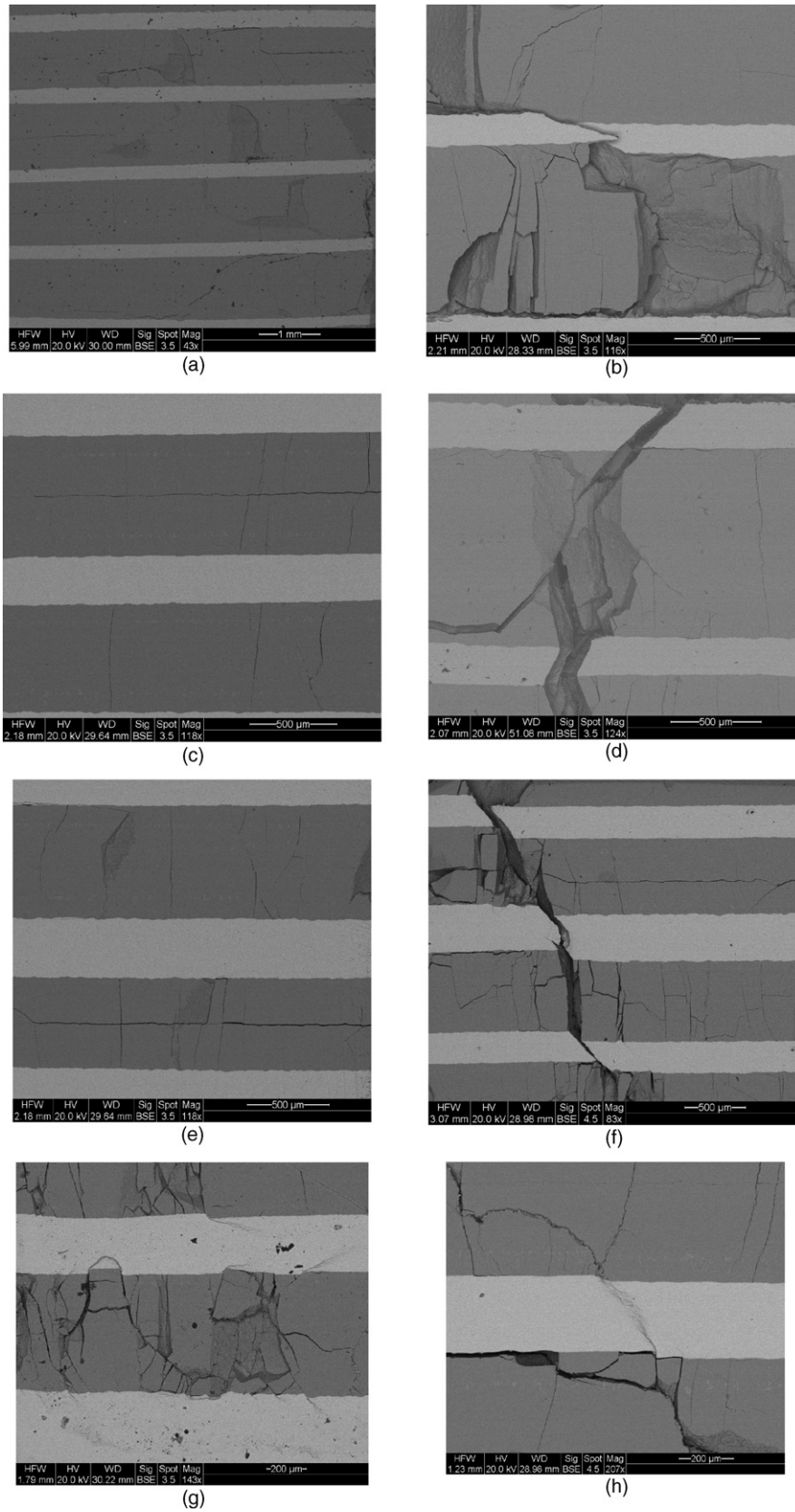


Fig. 14. SEM of MIL composites after quasi-static compression in perpendicular loading: (a) 14% Ti6Al4V, ~1% strain; (b) 14% Ti6Al4V, ~2% (failure); (c) 20% Ti6Al4V, ~1% strain; (d) 20% Ti6Al4V, ~2.8% (failure); (e) 35% Ti6Al4V, ~1% strain; (f) 35% Ti6Al4V, ~3.4% (failure); (g) 35% Ti6Al4V, ~2%; (h) 20% Ti6Al4V, ~2.5%.

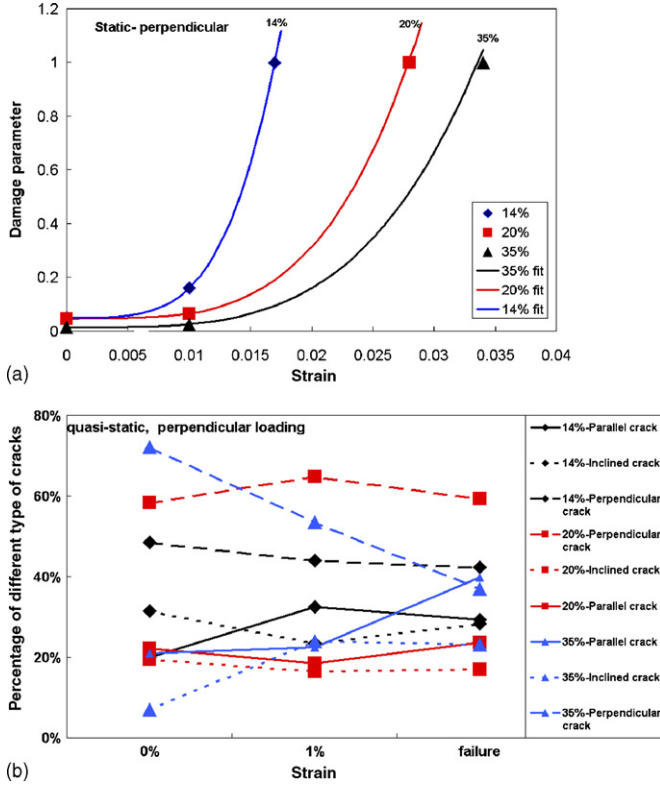


Fig. 15. Crack density and crack distribution for MIL composites with different strains after quasi-static compression in perpendicular loading: (a) damage parameter; (b) crack distribution.

interfaces. Comparing with quasi-static deformation, the Al_3Ti layers are much more fragmented and the $\text{Ti}_6\text{Al}_4\text{V}$ layers are largely segmented. Many parts of Al_3Ti (Fig. 16(h)) and even parts of the composites (Fig. 16(b)) were blown away upon impact, which makes the stresses concentrate faster in $\text{Ti}_6\text{Al}_4\text{V}$ layers where the Al_3Ti are absent, and thus accelerates the process from the generation of shear bands to the failure of $\text{Ti}_6\text{Al}_4\text{V}$ by shear cracks. This is why very few shear bands are observed in dynamic tests. Once one layer of $\text{Ti}_6\text{Al}_4\text{V}$ fails, the rest $\text{Ti}_6\text{Al}_4\text{V}$ layers taking even more loadings fail consecutively.

Fig. 17 shows the damage parameter and crack distribution after dynamic deformation. It is seen that as the strains increase, the damage parameter in different volume fractions of $\text{Ti}_6\text{Al}_4\text{V}$ increases, and the increase accelerates approaching failure. The trend for 35% MIL composites is unusual because only specimens with $\sim 1.5\%$ strain were obtained and thus overestimated the damage parameter. In percentage terms (Fig. 17(b)), it shows that generally the concentrations of the perpendicular cracks decrease, and the concentrations of the parallel cracks increase, while the concentrations of the inclined cracks are stable. This means the parallel cracks along the middle of the Al_3Ti layers and delaminations along the interfaces are more popular in dynamic perpendicular deformation than in quasi-static perpendicular deformation.

Fig. 18 compares the crack density at $\sim 1\%$ strain and failure after dynamic and quasi-static loading in perpendicular direction. It shows the similar trend as in parallel direction.

3.3. Effect of damage on elastic modulus

The damage in the MIL composites has a considerable effect on the elastic modulus. An expression developed by O'Connell and Budiansky [34] is used and modified to model the effect:

$$\frac{E}{E_0} = 1 - \frac{16(10 - 3\nu)(1 - \nu^2)}{45(45 - \nu)} f_s \approx 1 - 1.63Na^3 \quad (5)$$

where N is the number of cracks per unit volume and a is the radius of a mean crack. E is the effective Young's modulus of the cracked material. E_0 is the Young's modulus of uncracked material and for MIL composite, it is equal to in parallel direction

$$E_0 = V_{\text{Ti}}E_{\text{Ti}} + V_{\text{Al}_3\text{Ti}}E_{\text{Al}_3\text{Ti}} \quad (6)$$

and in perpendicular direction

$$\frac{1}{E_0} = \frac{V_{\text{Ti}}}{E_{\text{Ti}}} + \frac{V_{\text{Al}_3\text{Ti}}}{E_{\text{Al}_3\text{Ti}}} \quad (7)$$

The definition of cracks used by O'Connell and Budiansky [34] differs from the one in Eq. (5). O'Connell and Budiansky considered circular crack with radius of a (Fig. 19(a)), while we consider rectangular cracks with the smaller side equal to $2a$ and the larger side equal to the thickness of the specimen (Fig. 19(b)). These asymmetric cracks are produced by the unimpeded crack growth in Al_3Ti . In the O'Connell–Budiansky equation, Na^3 is a measure of the fraction of the material that is under the effect of the cracks, and we modify this equation by replacing Na^3 by the fraction of the material under the effect of rectangular cracks in Al_3Ti :

$$Na^3 = \frac{m\pi a^2 t}{At} = D \quad (8)$$

where m is the total number of cracks, a the half of the crack size in Al_3Ti , t the thickness of Al_3Ti and A is the surface area of MIL specimen. Substituting Eq. (8) into Eq. (5)

$$E = E_0[1 - 1.63D] = E_0[1 - 1.63(D_0 + k\varepsilon^n)] \quad (9)$$

Since $E = (d\sigma/d\varepsilon)$, the calculated stress–strain relation can be obtained:

$$\begin{aligned} \sigma &= \int_0^\varepsilon E d\varepsilon = \int_0^\varepsilon E_0[1 - 1.63(D_0 + k\varepsilon^n)] d\varepsilon \\ &= E_0 \left[(1 - 1.63D_0)\varepsilon - \frac{1.63k\varepsilon^{n+1}}{n+1} \right] \end{aligned} \quad (10)$$

The failure stress occurs at $d\sigma/d\varepsilon = 0$, i.e., the onset of softening. This corresponds to

$$\frac{d\sigma}{d\varepsilon} = E_0[(1 - 1.63D_0) - 1.63k\varepsilon^n] = 0 \quad (11)$$

Thus,

$$\begin{aligned} \varepsilon_{\text{failure}} &= \left(\frac{1 - 1.63D_0}{1.63k} \right)^{1/n} \quad \text{and} \\ \sigma_{\text{failure}} &= E_0 \left[\frac{n(1 - 1.63D_0)}{n+1} \left(\frac{1 - 1.63D_0}{1.63k} \right)^{1/n} \right] \end{aligned} \quad (12)$$

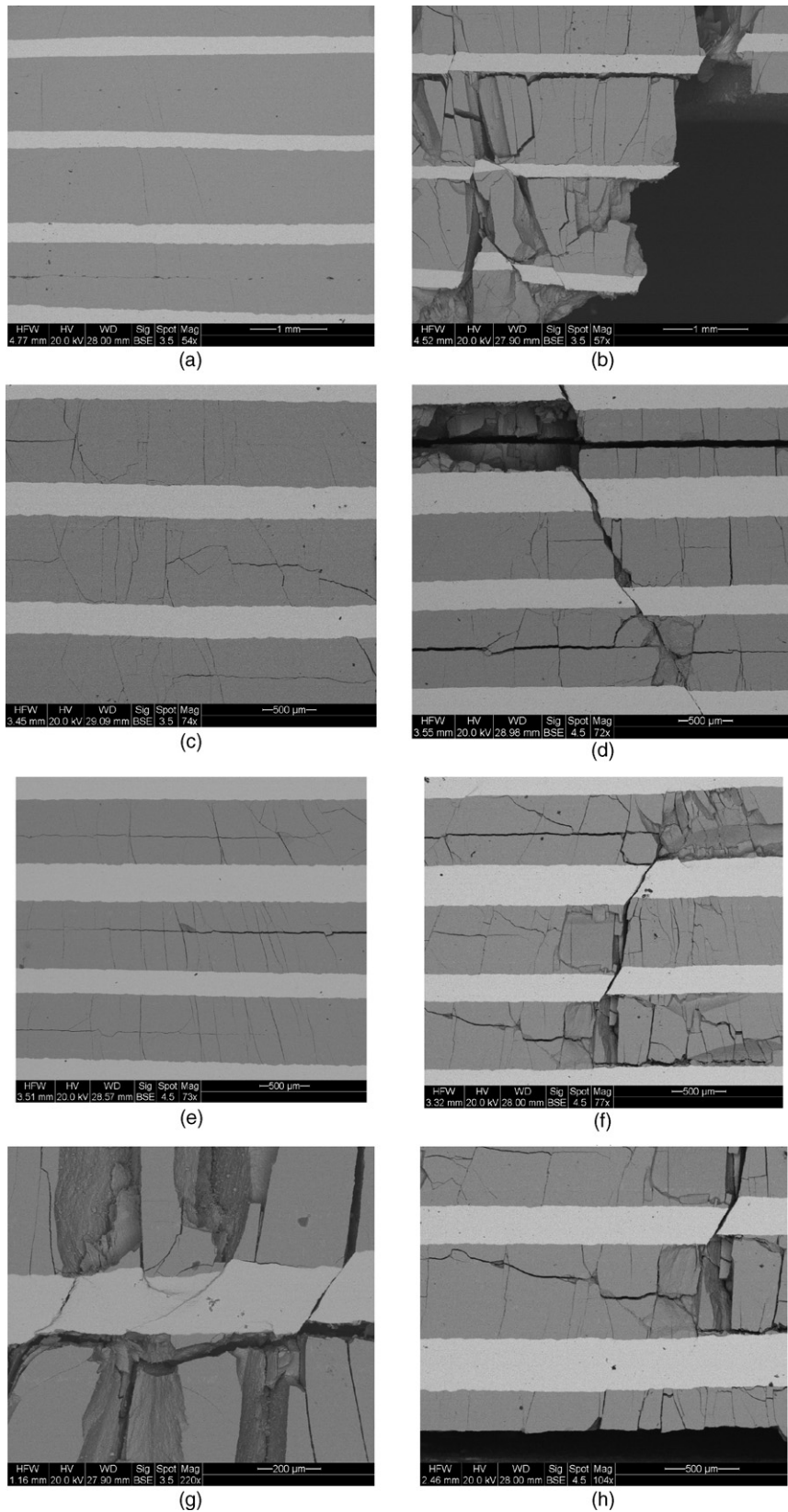


Fig. 16. SEM of MIL composites after dynamic compression in perpendicular loading: (a) 14% Ti6Al4V, ~1% strain; (b) 14% Ti6Al4V, ~2.2% (failure); (c) 20% Ti6Al4V, ~1% strain; (d) 20% Ti6Al4V, ~3.1% (failure); (e) 35% Ti6Al4V, ~1.4% strain; (f) 35% Ti6Al4V, ~3.5% (failure); (g) 14% Ti6Al4V, ~2.2%; (h) 35% Ti6Al4V, ~3.5% (failure).

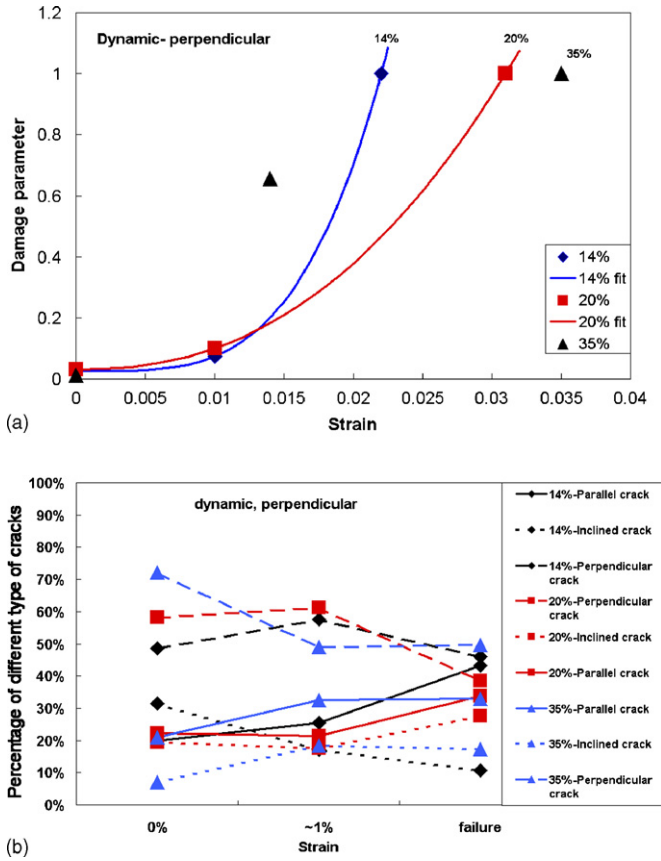


Fig. 17. Crack density and crack distribution for MIL composites after dynamic compression in perpendicular loading: (a) damage parameter; (b) crack distribution.

Figs. 20 and 21 compare the calculated and experimental elastic relations in parallel and perpendicular directions for quasi-static and dynamic deformation. In quasi-static deformation, the calculated elastic relation compares well with the experimental data at small strains and only deviates when approaching

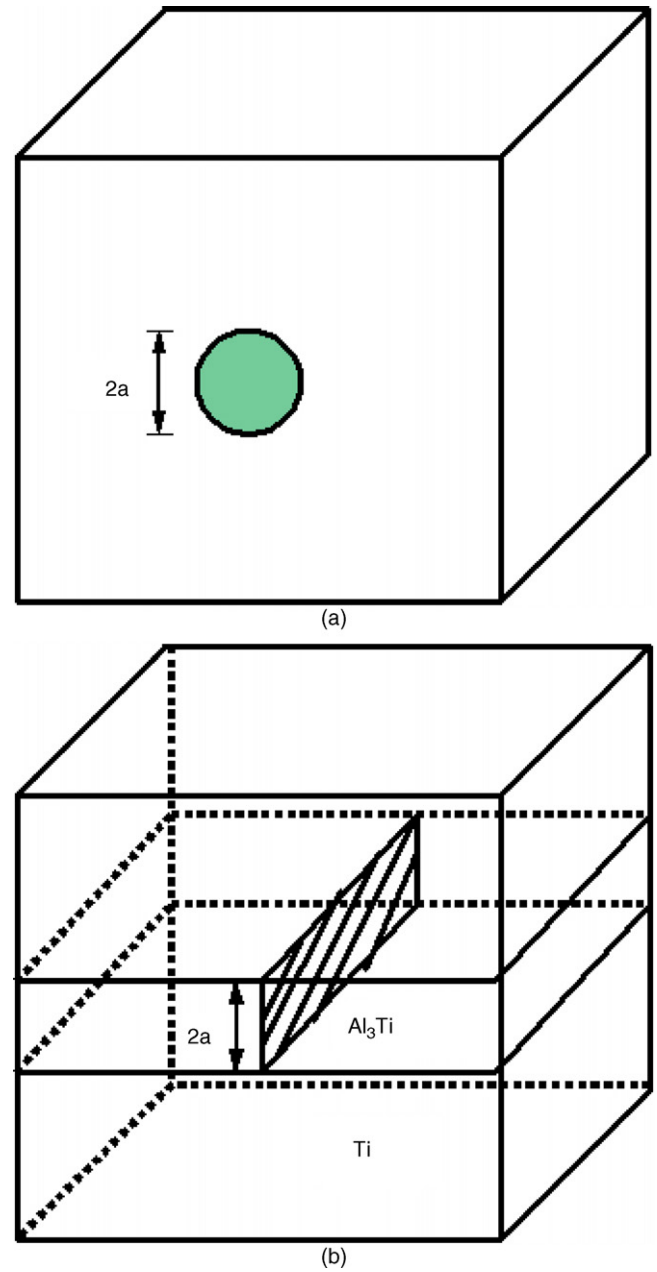


Fig. 19. Schematic of crack shapes: (a) O'Connell and Budiansky crack; (b) MIL crack.

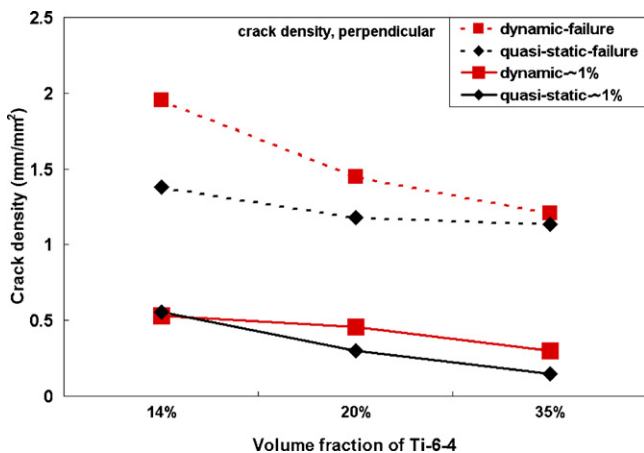


Fig. 18. Crack density comparison in 1% and failure strain after the dynamic and quasi-static loading in perpendicular direction.

failure (Figs. 20(a) and 21(a)). On the other hand, in dynamic deformation, the calculated values deviate from the experimental data from the beginning and such deviation intensifies as strain increases (Figs. 20(b) and 21(b)). Mathematically, in dynamic deformation, the material parameters k and n are larger than those in the quasi-static deformation, and according to Eq. (11), they decrease the elastic slope. Physically, the materials undergo some extreme situations and therefore, the calculation is less predictable in dynamic loading. One possible reason for this is that cracks continue to grow under unloading, in the dynamic case; therefore, the measured density is higher than the one existing under loading.

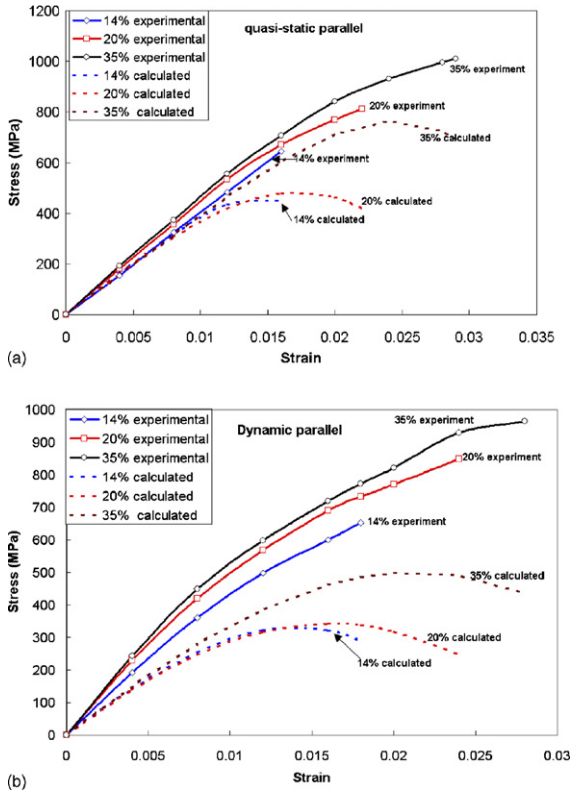


Fig. 20. Comparison of calculated and experimental stress–strain relation for MIL composites in parallel loading direction: (a) quasi-static; (b) dynamic.

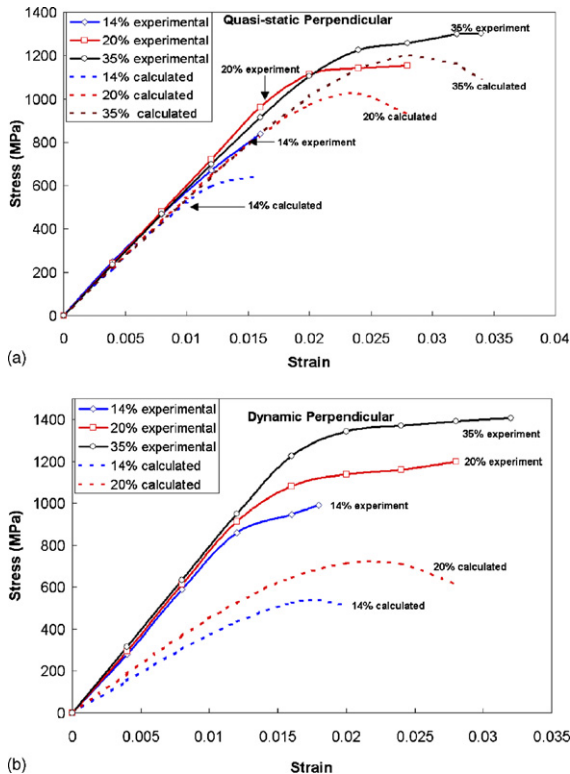


Fig. 21. Comparison of calculated and experimental stress–strain relation for MIL composites in perpendicular loading direction: (a) quasi-static; (b) dynamic.

4. Conclusions

The crack propagation and damage evolution in the MIL composites have been investigated by testing under different loading directions, to different strains, at different strain rates and for different volume fractions of Ti6Al4V. The following conclusions were drawn:

1. The cracks in the as-processed MIL composites can be classified into three categories: parallel to the interface, perpendicular to the interface and 45° inclined to the interface.
2. The crack densities measured for the as-processed 14%, 20% and 35% MIL composite are 0.321, 0.255 and 0.137 mm/mm^2 , respectively.
3. The concentrations of parallel cracks for MIL composites with different composition vary consistently: the concentration of perpendicular cracks increases from 49% (14% Ti6Al4V) to 72% (35% Ti6Al4V), while the concentration of inclined cracks decreases from 31% (14% Ti6Al4V) to 7% (35% Ti6Al4V).
4. The specimens tested in the parallel direction failed by delamination along the interfaces, cracking along the middle of the Al_3Ti layers, and buckling of Ti6Al4V. After dynamic deformation, the specimens were much more fragmented than after quasi-static deformation, and most Al_3Ti is comminuted and blown away upon impact.
5. The specimens tested in the perpendicular direction failed by shear, delamination along interface and cracking along the middle the Al_3Ti layers. As in the parallel direction, the specimens after dynamic deformation are much more fragmented than those after quasi-static deformation.
6. The crack density was measured using optical microscopy for all testing conditions and converted to a damage parameter, D . Generally, the damage parameter under dynamic deformation is higher than that in quasi-static deformation, for the same strain. The damage parameter increases with increasing strain, but decreases with increasing volume fraction of Ti6Al4V. D was found to increase from ~ 0.018 in the as-processed condition (D_0) to ~ 1 at failure.
7. The evolution of the elastic modulus was calculated and compared with the experimental results. It is found that the calculated elastic modulus in quasi-static deformation matches the experimental results well using the increase in microcracking through a modified O'Connell–Budiansky equation. The equation also enables the estimate of the compressive strength, which is the stress when $d\sigma/d\varepsilon = 0$. The results are in good agreement with experiments for quasi-static deformation. For dynamic deformation, the predicted elastic modulus is considerably lower than the measured values. This is interpreted as follows: microcrack growth is proceeding during and after compressive loading, so that the measured values reflect post-deformation growth during specimen unloading.

Acknowledgements

Help from Dr. Ma, Jing Cai, Tom Phillips and Evelyn York (Scripps Institution of Oceanography) in specimen preparation,

mechanical tests and SEM is greatly appreciated. This research was sponsored by DARPA through contract No. DAAD 19-00-1-0511.

References

- [1] D.R. Bloyer, V.K.T. Rao, R.O. Ritchie, Johannes Weertman Symposium, Proc. of a Symp., TMS, 1996, pp. 261–266.
- [2] D.R. Bloyer, V.K.T. Rao, R.O. Ritchie, Metall. Mater. Trans. A 29A (10) (1998) 2483–2496.
- [3] D.R. Bloyer, V.K.T. Rao, R.O. Ritchie, Mater. Sci. Eng. A A239–240 (1997) 393–398.
- [4] D.R. Bloyer, V.K.T. Rao, R.O. Ritchie, Mater. Res. Soc. Symp. Proc. 434 (1996) 243–248.
- [5] K.L. Hwu, B. Derby, Acta Mater. 47 (2) (1999) 529–543.
- [6] K.L. Hwu, B. Derby, Acta Mater. 47 (2) (1999) 545–563.
- [7] J. Rawers, K. Perry, J. Mater. Sci. 31 (13) (1996) 3501–3506.
- [8] L.S. Sigl, P.A. Mataga, B.J. Dalgleish, R.M. McMeeking, A.G. Evans, Acta Metall. 36 (4) (1988) 945–953.
- [9] P.A. Mataga, Acta Metall. 37 (12) (1989) 3349–3359.
- [10] K.T.V. Rao, W.O. Soboyejo, R.O. Ritchie, Metall. Trans. A 23A (8) (1992) 2249–2257.
- [11] M.F. Ashby, F.J. Blunt, M. Bannister, Acta Metall. 37 (7) (1989) 1847–1857.
- [12] F.W. Zok, C.L. Hom, Acta Metall. Mater. 38 (10) (1990) 1895–1904.
- [13] B.D. Flinn, C.S. Lo, F.W. Zok, A.G. Evans, J. Am. Ceram. Soc. 76 (2) (1993) 369–375.
- [14] B.J. Dalgleish, K.P. Trumble, A.G. Evans, Acta Metall. 37 (7) (1989) 1923–1931.
- [15] H.E. Deve, A.G. Evans, G.R. Odette, R. Mehrabian, M.L. Emiliani, R.J. Hecht, Acta Metall. Mater. 38 (1990) 1491–1502.
- [16] K.T.V. Rao, G.R. Odette, R.O. Ritchie, Acta Metall. Mater. 40 (2) (1992) 353–361.
- [17] M.C. Shaw, D.B. Marshall, M.S. Dadkhah, A.G. Evans, Acta Metall. Mater. 41 (1993) 3311–3322.
- [18] J. Heathcote, G.R. Odette, G.E. Lucas, R.G. Rowe, D.W. Skelly, Acta Mater. 44 (1996) 4289–4299.
- [19] D.R. Bloyer, K.T.V. Rao, R.O. Ritchie, Mater. Sci. Eng. A216 (1996) 80–90.
- [20] H.C. Cao, A.G. Evans, Acta Metall. Mater. 39 (1991) 2997–3005.
- [21] W.O. Soboyejo, F. Yea, L.C. Chena, N. Bahtishia, D.S. Schwartz, R.J. Lederich, Acta Mater. 44 (5) (1996) 2027–2041.
- [22] T. Li, F. Grignon, K.S. Vecchio, E.A. Olevsky, M.A. Meyers, Mater. Sci. Eng. A 374 (2004) 10–26.
- [23] G.R. Odette, B.L. Chao, J.W. Sheckherd, G.E. Lucas, Acta Metall. Mater. 40 (1992) 2381–2389.
- [24] R. Subramanian, J.H. Schneibel, Mater. Sci. Eng. A244 (1998) 103–112.
- [25] J.M. McNaney, R.M. Cannon, R.O. Ritchie, Acta Mater. 44 (12) (1996) 4713–4728.
- [26] Y. Huang, H.W. Zhang, Acta Metall. Mater. 43 (4) (1995) 1523–1530.
- [27] J.C. Rawers, D.E. Alman, Comput. Sci. Technol. 54 (4) (1995) 379–384.
- [28] J. Rawers, K. Perry, J. Mater. Sci. 31 (13) (1996) 3501–3506.
- [29] M.R. Fox, A.K. Ghosh, Mater. Sci. Eng. A259 (1999) 261–268.
- [30] D.J. Harach, K.S. Vecchio, Metall. Mater. Trans. A 32A (2001) 1493–1505.
- [31] A. Rohatgi, D.J. Harach, K.S. Vecchio, K.P. Harvey, Acta Mater. 51 (2003) 2933–2957.
- [32] K.S. Vecchio, JOM 57 (3) (2005) 25.
- [33] T. Li, M.A. Meyers, E. Olevsky, A. Olevsky, unpublished results, 2006.
- [34] R.J. O’Connell, B. Budiansky, J. Geol. Res. 79 (1974) 5412.